Article submitted to: High Power Laser Science and Engineering, 2023 *May 18, 2023*

Measurements of Plasma Density Profile Evolutions with Channel-guided Laser

Tong Yang[1,2], Zhen Guo[1,2], Yang Yan[1,2], Minjian Wu[1,2], Yadong Xia[1,2], Qiangyou He[1,2], Hao Cheng[1,2], Yuze Li[1,2], Yanlv Fang[1,2], Yanying Zhao[1,2,3], Xueqing Yan[1,2,3], and Chen Lin*[1,2,3]

[1] *State Key Laboratory of Nuclear Physics and Technology, and Key Laboratory of HEDP of the Ministry of Education, CAPT, Peking University, Beijing, 100871, China*
[2] *Beijing Laser Acceleration Innovation Center, Huairou, Beijing,101400, China*
[3] *Institute of Guangdong Laser Plasma Technology, Baiyun, Guangzhou,510540, China*

Abstract
Discharged capillary plasma channel has been extensively studied as a high gradient particle acceleration and transmission medium. A novel measurement method of plasma channel density profiles has been employed, where the role of plasma channels guiding the advantages of laser has shown strong appeal. Here, we have studied the high order transverse plasma density profile distribution using channel-guided laser, and made detailed measurements of its evolution under various parameters. The paraxial wave equation in a plasma channel with high-order density profile components is analyzed, and the approximate propagation process based on the Gaussian profile laser is obtained on this basis, which agrees well with the simulation under phase conditions. In the experiments, by measuring the integrated transverse laser intensities at the outlet of channels, the radial quartic density profiles of plasma channels, have been obtained. By precisely synchronizing the detection laser pulses and the plasma channels at various moments, the reconstructed density profile shows an evolution from the radial quartic profile to the quasi-parabolic profile, and the high-order component is indicated as an exponential decline tendency over time. Factors affecting the evolution rate were investigated by varying the incentive source and capillary parameters. It can be found that discharge voltages and currents are positive factors quickening the evolution, while electron-ion heating, capillary radii and pressures are negative ones. One plausible explanation is that quartic profile contributions may be linked to plasma heating. This work helps to understand the mechanisms of the formation, evolutions of the guiding channel electron density profiles and their dependences on the external controllable parameters. It provides support and reflection for the physical research on discharged capillary plasma and optimizing plasma channels in various applications.

Keywords: Channel-guided laser, discharge capillary, plasma density profile.

1. Introduction

Laser plasma accelerators (LPAs)[1,2] can produce electric acceleration fields of the order of tens to hundreds of GV/m[3,4], making them attractive as compact particle accelerators. This mechanism makes it is possible to reduce the distance required to generate GeV-level electron beams from kilometers to centimeters[5–8]. Thus, it promises to increase the availability of the important resource, highly relativistic, high-brightness electron beams as an essential tool for fundamental and application research, at significantly reduced size and cost. Over the past decade, milestone experiments have verified key principles of LPA and the possibility to generate high-brightness beams, featuring electron bunches of low emittance[9,10], multi-femtosecond length, and kiloampere peak current[11–13]. These results show that LPAs are, in principle, capable of generating electron beams with competitive beam quality. Especially, significant progress has been made on LPAs, yielding quasi-monoenergetic electron beams[14–16] with the highest energy record on three steps from 1 GeV to 7.8 GeV by ultra-intense laser pulse guided in multi-cm-long gas-filled capillary discharge waveguides[6–8]. In the preformed plasma density channels, the propagation distance of a laser pulse can reach tens of times larger than the Rayleigh length. Experimental studies and solutions of an efficient approach to coupling laser pulses with high mode quality to a preformed plasma channel waveguide have made important contributions to advancing the field of LAPs.

For the application, it is highly desirable that the laser pulse should propagate extended distances (many Rayleigh

Correspondence to: Peking University, Beijing, 100871.
Email: lc0812@pku.edu.cn

10.1017/hpl.2023.50

lengths) at high intensity. In the absence of an optical guiding mechanism, the propagation distance is limited to approximately a Rayleigh (diffraction) length $Z_R = \pi r_0^2/\lambda$, where λ is the laser wavelength and r_0 is the laser spot size at focus. High intensities require a tight focus and, consequently, a relatively short Rayleigh length. However, the limitation may be breached up to over distances of several centimeters, utilizing preformed plasma density channels. An approach for creating density channels is to use slow gas-filled capillary discharges[17]. In the device, instead of auxiliary laser, a current pulse is passed through a capillary with an inner diameter of a few hundred microns and scaling length of several even tens of centimeters, prefilled with gas at a pressure of tens to hundreds of millibar. The current pulse has a peak of a few hundred amperes and a duration of the order of hundreds of nanoseconds. Capillary discharges have been used to create straight or curved plasma channels, in which laser pulses have been guided over many Rayleigh lengths[17–24]. Gas-filled capillary discharge waveguides offer a number of advantages in guiding intense laser pulses, such as low transmission and coupling losses. This is a mainstream more popular stabilization method with a parabolic density profile, which allows the propagation of Gaussian laser pulses with constant a matched spot size radius[25,26].

Furthermore, advanced concepts with capillary discharges have demonstrated novel injection techniques[27–31], the generation of plasma-driven x-ray pulses[32,33], synchrotron radiations[34] and high-harmonic[35], cascade acceleration schemes[36–38], energy dechirper[39–41], and the transport of LPA electron[35,42–50] and proton beams[51,52] as novel active plasma lenses (APLs). In particular, APLs have focus gradient up to several kT/m. Combined with the laser plasma acceleration, it hopes to realize the miniaturization of particle accelerators. But the quality of beam transports would be degraded in APLs with non-uniform current densities, which are closely related to the plasma electron density profiles. And for all the applications above, gas-filled capillaries offer the ability to continuously tune the plasma pressure and long device lifetimes. In addition, in the case of gas-filled capillaries, the plasma channel may be fully ionized, which minimizes spectral or temporal distortion. It is helpful for sensitivity of measurement. For both channel-guided laser and beams, the measurements of plasma channel density profiles are important evidence.

In general, refractive guiding of optical pulses can occur when the transverse (radial) profile of the index of refraction η is peaked along the propagation axis. A plasma column or channel with a transverse electron density minimum on the axis has $\partial\eta/\partial r < 0$ and thus produces the desired refractive index profile for guiding, where r is the radial component. Specifically, a plasma channel with a radially parabolic density profile of the form $n(r) = n_0 + \Delta n r^2/r_0^2$ can guide a laser pulse of spot size r_0 provided the channel depth satisfies $\Delta n = \Delta n_c$, where n_0 is the density in axis, $\Delta n_c = 1/\pi r_e r_0^2$ is the critical channel depth and $r_e = e^2/\left(4\pi\varepsilon_0 m_e c^2\right) = 2.8 \times 10^{-15}$ m is the classical electron radius[53,54]. It has been shown that the presence of the plasma channel leads to betatron oscillations of the laser spot, which allows the laser to be confined close to the axis of channels. There is a lot of research work[55–61] devoted to analyzing the optical guiding of laser pulses in plasma channels, e.g., solving the paraxial wave equation with nonlinear source terms using the well-known source-dependent expansion (SDE) method[62,63]. Particularly, previous research built the basis of quasi-matched spots for higher-order density profiles beyond parabolic ones[64], the laser propagation with a mismatched spot has been analyzed[65], and matched Laguerre–Gaussian modes in high-order plasma channels has been proved[66].

In the gas-filled capillary discharge, the plasma channel is formed by the temperature profile during discharge, which is higher in the center as a result of the Ohmic heating effect of plasma and drops radially because the heating is balanced by heat conduction to the capillary wall[67,68]. Measurements of the transverse electron density profile in a hydrogen-filled device have shown that a quasi-parabolic plasma channel is indeed formed[69]. In the outer edge of a plasma channel, the density profile described by a parabola alone is not sufficient, because the quasi-thermal equilibrium conditions may be violated due to large temperature gradients and violent particle collisions. It is worth paying attention to the impact of experimental non-ideal parabolic density distributions on applications, since the density dominates the plasma response time, self-injection threshold, accelerating field strength, electron beam dephasing length[3], beam-driven wakefield effects[44], the spatial distribution of discharge current density, phase space development of charged particles during transport[43,44] and radiation generating phase matching conditions[70].

Different application scenarios need to adapt to the density distribution under different time windows. For instance, the time window of the plasma channel as the best matching guide waveguide is only less than tens of nanoseconds. Knowledge of the plasma density profile evolution is of critical importance to optimizing the performance of the channel. Current techniques for measuring the density channel profiles in a gas-filled capillary discharge waveguide are inadequate. Longitudinal interferometry experiments with the Mach-Zehnder interferometer require the capillary length to be less than a few millimeters, resulting in measurement error associated with end effects[71–73] . Transverse interferometry measurements require capillaries that are square necessitating strong assumptions about the symmetry of the profile[74–79] and flat optical side windows are necessary to provide the optical path. The well-known spectroscopic method using the Stark broadening effect loses the ability to spatially resolve[80–82]. An alternative way to detect

https://doi.org/10.1017/hpl.2023.50 Published online by Cambridge University Press

the plasma density, based on the shock waves produced by gas discharge in a capillary[83] yields only integrated axial distribution information and must be calibrated by other methods. Spot size measurements at the output of the capillary have also been used to deduce channel depth[84,85], but this technique requires several plasma channels with different lengths while keeping other parameters consistent. Another method employs the observation of Raman shifts in the guided laser spectrum, but this requires a high laser power[86,87]. The group velocity delay[88] of a laser pulse and the common-path two-color interferometer[89,90] can only be correlated with the on-axis plasma density. Extensive research has been carried out on more details on the shape of the channel and accurate diagnostics of paraxial plasma channel depth by the method of measuring laser centroid oscillations[91] and the quartic density distribution of plasma channels is first introduced into measurement research[91,92]. On the other hand, in order to assist the development of this channel, important simulations[67,68,93] of the plasma dynamics of a hydrogen-filled capillary discharge have been studied, to understand the mechanisms by which the guiding electron density profile is formed and how its properties depend on the external, controllable parameters.

In this paper, we report the measurement of the temporal evolution of the electron-density profile, in particular, including marginal higher-order distributions in a gas-filled discharge capillary by distinguishing channel-guided laser mode quality. Adopting of a collimated laser eliminates the influence of the divergence angle of the probe laser to ensure the accuracy. The intensity was kept low ($< 10^{14}$ W/ cm^{-2}) in these experiments so that nonlinear effects such as self-focusing, wake formation and hosing could be neglected and the plasma properties measured in a straightforward way. This method relies on the fact that the radial density profiles in gas-filled capillary discharge waveguides mainly depend on the three parameters, the diameter of a capillary, the discharge current profile and the filling gas pressure, in absence of the longitudinal flow. We shall present the method from three aspects, including theory in Sec.2, simulations in Sec.3 and experiments in Sec.4 and Sec.5. The work is aimed to contribute to the in-depth study of the evolution mechanism and properties of plasma channels and to implement optimizations in a variety of applications.

2. Heuristic Theory of channel-guided propagation

In this paper, the mathematical model for describing laser pulse evolution is based on the wave equation

$$\left(\nabla^2 - \frac{1}{c^2}\frac{\partial^2}{\partial t^2}\right) E = k^2\left(1-\eta_r^2\right)\hat{E} \tag{1}$$

where $E = \mathrm{Re}\left[\hat{E}e^{ik(z-ct)}\right]$ is transverse electric field of the laser, $\hat{E}(r,z,t)$ is the slowly varying amplitude envelope, $\omega = ck = 2\pi/\lambda$ is the laser frequency, k is the laser wave number, λ is the laser wavelength, c is the speed of light in a vacuum, t is time independent variable, η_r is the index of refraction of the medium, and $\left|1-\eta_r^2\right| \ll 1$ is assumed. Here, η_r is generally a nonlinear function of the medium density profile.

$$\eta_r = 1 - \frac{k_p^2(r)}{k^2} \tag{2}$$

where k_p is the plasma wave number. In the following, it will be assumed that η_r is real i.e., dissipative effects such as collisions and absorption will be neglected. The following analysis is carried out under the axisymmetric cylindrical coordinate system, with z the axial propagation direction, and r radial component.

$$\nabla_\perp^2 = \nabla^2 - \frac{\partial^2}{\partial z^2} \simeq \frac{1}{r}\frac{\partial}{\partial r}\left(r\frac{\partial}{\partial r}\right) \tag{3}$$

where $\partial^2/\partial z^2$ is typically small which will be neglected.

The propagation of an ultrashort laser pulse in a preformed plasma channel will be considered. Propagation is considered in the limits of low power $P/P_c \ll 1$ and low intensity $a_0^2 \ll 1$, such that nonlinear effects (e.g., relativistic self-focusing) can be neglected and the density channel can be assumed unaffected by the laser pulse, where P is the laser power, P_c is the critical power for relativistic self-focusing and a_0 is the laser relativistic intensity. The starting point for describing laser pulse evolution in plasma is the linear paraxial wave equation[94] for the transverse component of the laser field, which can be written in the form

$$\left(\nabla_\perp^2 + 2ik\frac{\partial}{\partial z}\right)\hat{E} = k_p^2(r)E \tag{4}$$

where $k_p^2(r) = k_{p0}^2 n(r)/n_0$, $k_{p0} = \omega_{p0}/c$ is the plasma wave number, $\omega_{p0} = \sqrt{n_0 e^2/(\varepsilon_0 m_e)}$ is the plasma frequency and n_0 is the electron plasma density on the central axis ($r = 0$), e is the elementary charge, ε_0 is the vacuum permittivity, m_e is the electronic quality in an international system of units and $n(r)$ is the radial distribution of plasma channel density will introduce below.

To analyze the behavior of the pulse radius, consider the local normalized-intensity-weighted mean-squared radius $\langle r^2\rangle$ defined by

$$\langle r^2\rangle = \frac{\int_0^\infty r^3\left|\hat{E}\right|^2 dr}{\int_0^\infty r\left|\hat{E}\right|^2 dr} \tag{5}$$

We say that a laser propagating in a plasma channel satisfies a quasi-matched propagation condition if its second order $\partial^2\langle r^2\rangle/\partial z^2$ remains zero. Plasma channels focus laser pulses due to a radially varying refractive index. Self-steepening and depletion have been neglected to simplify

https://doi.org/10.1017/hpl.2023.50 Published online by Cambridge University Press

the analysis of the problem. The matched spot size w_m can be obtained from the radial electron density distribution according to [64]

$$8\pi r_e \int_0^\infty \left[n(r) \left(\frac{2r^2}{w_m^2} - 1 \right) e^{-\frac{2r^2}{w_m^2}} \right] r dr - 1 = 0 \qquad (6)$$

Equation.6 gives general matched spot size for applicable densities, besides parabolic density profiles. High-order contributions should be introduced for a complete depiction of density profiles. One model provides an excellent description as shown in Figure.1 with quartic terms of the outer edge density profile for $|r| > 2w_m$ as [92]

$$n(r) = n_0 + \frac{1 - E_\Psi}{\pi r_e w_m^4} r^2 + \frac{E_\Psi}{2\pi r_e w_m^6} r^4 \qquad (7)$$

where E_Ψ is a scaling factor for the relative contributions of the quadratic distribution (r^2 term) and the quartic distribution (r^4 term), and r_{ch} is the maximum radius of the outer edge of the channel. Considering a specific plasma evolution over time, the average density $\langle n \rangle = \int_0^{r_{ch}} n(t) r dr / r_{ch}^2$ is approximately conserved, which would be discussed in the Sec. 5. The channel can guide multiple matched laser sizes at various moments with various E_ψ, as the black and red lines shown in Fig.1. When it comes to a specific matched spot, multiple matched channels can be produced with various E_ψ and $\langle n \rangle$, as the black and blue lines shown in Fig.1. In the description of channel-guided laser physics, the parameters E_ψ, w_m and $\langle n \rangle$ are closely related. Equation. 7 can be rewritten into an equivalent form

$$n(r) = n_0 + \Delta n_{r2} \frac{r^2}{r_{ch}^2} + \Delta n_{r4} \frac{r^4}{r_{ch}^4} \qquad (8)$$

For $E_\Psi < 1$ and $r^2 \ll r_{ch}^2$, a rough approximation can be taken

$$n(r) \simeq n_0 + \Delta n_{ch} \frac{r^2}{r_{ch}^2} = n_0 + \Delta n_{r2} \left(1 + \frac{\delta \Delta n_{r2}}{\Delta n_{r2}} \right) \frac{r^2}{r_{ch}^2} \qquad (9)$$

where $\delta \Delta n_{r2} = \Delta n_{r4} r^2 / r_{ch}^2 \ll \Delta n_{r2}$.

Approximate forms for the envelope equations describing laser pulse evolution i.e., a solution to the paraxial wave equation Eq.4 can be found by the method through heuristic theory, considering a Gaussian model laser beam with form

$$E = E_s \mathrm{e}^{i\theta - (1 - i\,\varphi_G) \frac{r^2}{w^2}} \qquad (10)$$

where E_s, φ_G, w, θ represent the amplitude, curvature, spot size and phase shift. Analysis of the paraxial wave equation Eq.4 with an index of refraction of an ideal radially parabolic density profile form indicates that the spot size w evolves

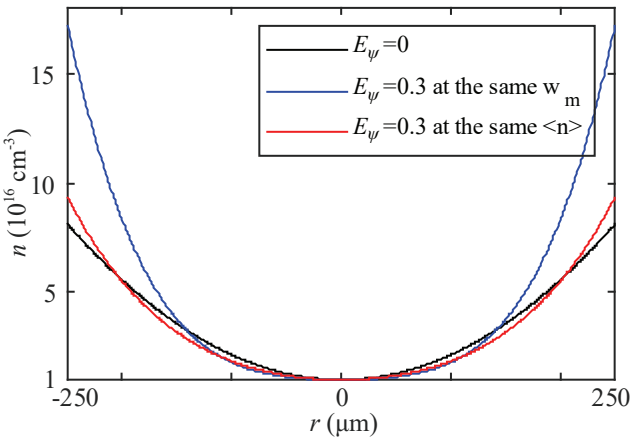

Figure 1. Calculated the plasma electron density profiles $n(r)$ as a function of radial position r with axis density $n_0 = 1 \times 10^{16}$ cm^{-3} and matched spot size $w_m = 100$ μm for a parabolic channel (black line) compared with a channel with an r^4 component with $E_\Psi = 0.3$ at the same w_m (blue line) and a channel at the same $\langle n \rangle$ (red line), respectively.

according to Heuristic theory [94]

$$\frac{\partial^2 w}{\partial z^2} = \frac{4}{k w^2} \left(1 - \frac{w^4}{w_m^4} \right) \qquad (11)$$

where the matched beam spot size w_m is given by

$$w_m^4 = \frac{r_{ch}^2}{\pi r_e \Delta n_{ch}} \qquad (12)$$

Note that the high-order density profile component contributes to a mismatched spot as mathematical equivalence.

$$w_m = w_{mM} \left(1 - \frac{1}{4} \frac{\delta \Delta n_{r2}}{\Delta n_{r2}} \right) = w_{mM} + \delta w_m \qquad (13)$$

where $w_{mM} = \sqrt[4]{r_{ch}^2 / (\pi r_e \Delta n_{r2})}$ is the matched spot size of paraxial density profile. The laser evolution from paraxial wave equation Eq.4, with the initial (at $z = 0$) conditions $\varphi_G = 0, \theta = 0, \partial w / \partial z = 0$, is given by [65]

$$E = E_0 \left[1 - \frac{\delta w_m}{w_m} \left(1 - \frac{2r^2}{w_m^2} \right) \mathrm{e}^{-ik_{os} z} \right] e^{-\frac{r^2}{w_m^2}} \qquad (14)$$

We can get the radial intensity profile evolution

$$\begin{aligned} I &= E E^* \\ &= E_0^2 \left\{ 1 + [\Psi \chi (1 - \chi)]^2 - 2\Psi \chi (1 - \chi) \cos k_{os} z \right\} e^{-\chi} \end{aligned} \qquad (15)$$

where $k_{os} = 4 / \left(k w_m^2 \right)$ is the betatron wave number and $\chi = 2r^2 / w_m^2$. One coefficient can be defined

$$\Psi = \frac{1}{8} \frac{\Delta n_{r4}}{\Delta n_{r2}} \sqrt[4]{\pi r_e \Delta n_{r2} r_{ch}^2} \qquad (16)$$

https://doi.org/10.1017/hpl.2023.50 Published online by Cambridge University Press

to denote the rate of contributions of r^4 term to that of r^2 term.

The above proof illustrates the impact of r^4 term of the electron density on laser intensity distribution in accordance with Eq.15, which is obviously different from the Gaussian model within ideal parabolic density profiles. The employed centroid displacement technique[91] can provide parabolic plasma channel shape information, i.e., Δn_{r2} intuitively. But without an explicit expression, the measurement of Δn_{r4} generally relies on an iterative agreement between experimental data and the simulation process. In addition, the intensity distribution measurement as a novel method can get the off-axial density Δn_{r4} at the channel outlet via fitting the equation Eq.15 for fixed z.

3. Simulation of laser propagation in plasma channels

Actually, it is important to specify the laser mode injected into the plasma channel. In our experiments, the collimated laser used with a particularly large Z_R can be approximated as a plane wave, due to its spot size significantly larger than the radius of the plasma channel. However, it is usually disregarded that the diffraction shaping effect on the pulse wavefront by the electrode hole and capillary wall from the electrode surface to the front end of the plasma channel, because of the gas inlet position[69]. We implemented an cylindrical 2D-vector integral transform[95] calculation in cylindrical coordinates to approximately explain the infinite diffraction propagation by a ideal scattering boundary (corresponding a electrode and capillary wall) as shown in Figure.2 (a), where the data on the negative side of the radial axis is performed by mirroring. The method is efficient in dealing with diffraction but requires extremely high spatial resolution. Within limited computing resources, we set an initial plane wave electric field with a wavelength $\lambda = 1\ \mu$m and a spatial step of 0.1λ in a 50 μm $\times$ 600 μm $(r \times z)$ calculation domain. The result of the calculation offers proof that, for the propagation of laser in a capillary with $r_{ch} \gg \lambda$, at only a short distance z that satisfies the Fresnel condition[96]

$$\frac{z}{2r_{ch}} \geq \sqrt[3]{\frac{2r_{ch}}{\lambda}} \tag{17}$$

the wavefront can be represented approximately as a Gaussian mode

$$E = E_0 \frac{2J_1(x)}{x} \simeq E_0 \mathrm{e}^{-\frac{r^2}{w^2}} \tag{18}$$

as shown in Fig.2 (b), where $x = x_{10} r/r_{ch}$, J_1 is the first-order Bessel function and x_{10} is the first zero point of $J_1(x)$. In a vacuum, the edge density of a discharge capillary plasma channel drops steeply[80], and the refractive index change of the gas outside the electrode is over two orders of magnitude smaller than that of the plasma[97]. The model could be regarded as the input consistent with the quasi-Gaussian mode in Eq.16 at $z = 0$.

In order to check the applicability of the aforementioned

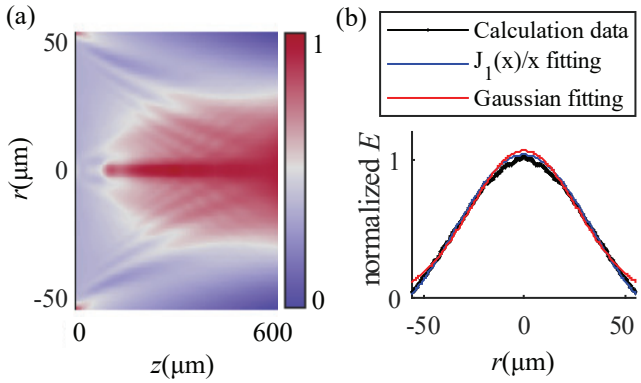

Figure 2. (a) The cylindrical 2D-vector integral transform calculation result of a input plane wave electric field E with wavelength $\lambda = 1\ \mu$m diffraction propagation by a ideal scattering boundary in a 50 μm $\times$ 600 μm $(r \times z)$ domain, where the data on the negative side of the radial axis is performed by mirroring. (b)The normalized transverse E profile at $z = 500\ \mu m$ from calculation data (black line) and fitting the profile with the theoretical function $J_1(x)/x$ (blue line) and the approximate Gaussian function (red line) for the channel-guided laser requirement, respectively.

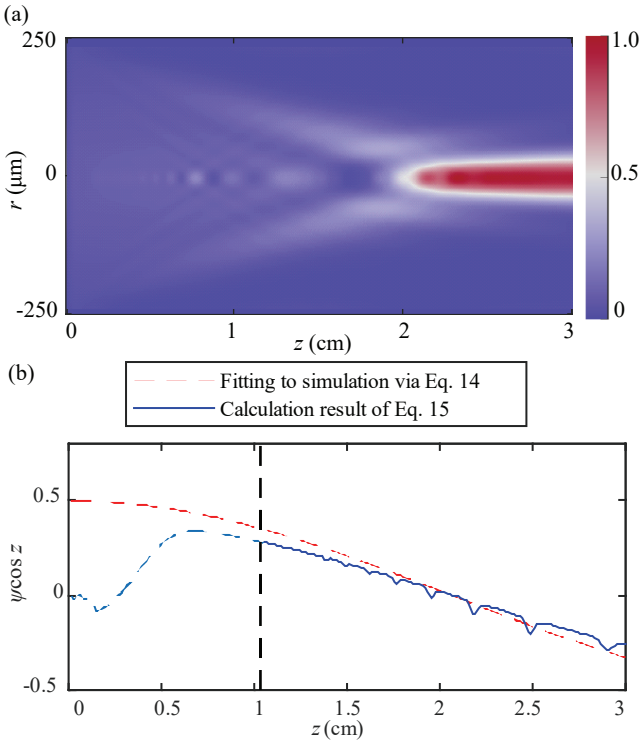

Figure 3. (a) The cylindrical PIC simulation result of laser with wavelength $\lambda = 1\ \mu$m propagation in plasma with ideal matched spot size $w_{mM} = 100\ \mu$m and $E_\psi = 0.3$, where the data on the negative side of the radial axis is performed by mirroring. The simulation domain corresponds to plasma channel radius r=500 μm and length $L = 3$ cm. (b) The coupling parameter $\Psi \cos k_{os} z$ varying along $z-$direction between the fitting to the simulation data via Eq.15 at every z position in the solid blue line and the calculation values of Eq.15 based on the initial set simulation parameters in the broken red line. The two show good consistency after laser propagating 1.2 cm.

https://doi.org/10.1017/hpl.2023.50 Published online by Cambridge University Press

Table 1. Parameters for all experimental groups

Number	Voltage	Gas	Waveform Style	Diameter	Pressure	Decline Rate ς
1	15 kV	He	Style 3	500 μm	100 torr	12.06 μs^{-1}
2	20 kV	He	Style 3	500 μm	100 torr	15.43 μs^{-1}
3	25 kV	He	Style 3	500 μm	100 torr	16.51 μs^{-1}
4	28 kV	He	Style 3	500 μm	100 torr	20.96 μs^{-1}
5	15 kV	Ar	Style 3	500 μm	100 torr	12.92 μs^{-1}
6	20 kV	Ar	Style 3	500 μm	100 torr	17.85 μs^{-1}
7	25 kV	Ar	Style 3	500 μm	100 torr	18.61 μs^{-1}
8	28 kV	Ar	Style 3	500 μm	100 torr	24.00 μs^{-1}
9	20 kV	He	Style 1	500 μm	100 torr	5.72 μs^{-1}
10	18 kV	He	Style 2	500 μm	100 torr	9.28 μs^{-1}
11	20 kV	He	Style 1	300 μm	100 torr	34.47 μs^{-1}
12	20 kV	He	Style 1	700 μm	100 torr	5.29 μs^{-1}
13	20 kV	He	Style 1	500 μm	80 torr	20.41 μs^{-1}
14	20 kV	He	Style 1	500 μm	90 torr	14.52 μs^{-1}

heuristic theory introduced, we have performed cylindrical particle-in-cell (PIC) simulations by the Smilei[64] code. The simulated transport domain is 500 μm$\times$3 cm (corresponding channel radius 250 μm and length 3 cm) in the $y-z$ plane. The simulations consider a plasma channel with a density distribution via $y-$direction described as Eq.7 with ideal matched spot size $w_{mM} = 100$ μm and $E_\psi = 0.3$. According to the theory above, ones can be calculated that channel density depth $\Delta n_{r2} = 7.08 \times 10^{16}$ cm^{-3}, quartic density contribution $\Delta n_{r4} = 1.13 \times 10^{17}$ cm^{-3} and the coefficient $\Psi = 0.5002$. Initially t=0, a parallel laser with wavelength $\lambda = 1$ μm emits from origin z=0. The betatron wave number $k_{os} = 0.64$ cm^{-1} can be calculated.

One of the simulation results is given in Figure.3 (a). It is obvious that the laser evolves complex models due to introducing a quartic density profile contribution. We fitted the laser intensity profiles along z-direction based on the form of Eq.15. The regularity of the coupling parameter $\Psi \cos k_{os} z$ from fitting results is represented by the blue line in Fig.3 (b). And the numerical result calculated with the above paragraph values along z-direction is also shown in Fig.3 (b) by the broken red line. It can be found that the simulation data well agrees with the calculation from its parameters, when satisfied an approximate condition $k_{os} z \gtrsim \pi/4$. Fig.3 (b) shows this condition as a demarcation by a broken black line. The limitation must be pointed out that Eq.15 cannot describe the process from a mismatched spot to a quasi-matched spot. Therefore, the broken light blue line fitting with Eq.15 shown in Fig.3 is unphysical. The condition indicates that there is a limit distance for a parallel laser pulse evolving into the model described by Eq.15, which is related to the focusing ability of the plasma. Meanwhile, it is should be considered the betatron oscillation damps in a distance of $k l_\tau / k_{os}$[65], which is the upper limit of the capillary length, where l_τ is the laser pulse width. Under such constraints, we adopted discharged plasma in capillaries with channel depth on the order of 10^{17} cm^{-3} and 3-cm length in experiments.

4. Experimental setup and methods

Figure.4 (a) provides a schematic overview of the experimental setup. We used a laser probe pulse to characterize the plasma channel properties. Laser pulses with a wavelength of 798 nm and spot radius of 4 mm were produced by the front end of the new developed terawatt laser system in Peking University as an upgrade part of the Compact LAser Plasma Accelerator (CLAPA)[98]. Collimated laser pulses are exported to the experiment area through a 50:50 beam-splitter downstream of the regenerative amplifier. The pulse energy is <0.2 mJ which is low enough to not modify the channel profile.

The capillary is placed on a motorized hexapod stage which can help to precisely adjust the alignment between a capillary and collimated laser pulses which will affect the output laser profile. For this paper, the length of all used capillaries is 3 cm and the radii are 150 μm, 250 μm and 350 μm. The off-axis deviation can be reduced to 33 μrad by judging the concentricity of the continuous diffraction imaging at the exit for 3-cm long capillaries and further to 5 μrad by judging the concentricity of the laser spot in the presence of the plasma channel. The capillary bulk material was either sapphire (Al_2O_3) or a high temperature laminating (HTL) resin. The HTL resin as a novel 3D-print material is cheaper can be in a single piece and is easily mechanically machinable. Helium (He) and argon (Ar) two types of gas can be filled in the capillary respectively whose pressure can be controlled from 10 torr to 300 torr. For the system, the scaling law between the average plasma density and pressure measured from spectroscopy is $\langle n \rangle [\text{cm}^{-3}] = 2.57 \times 10^{15} \cdot P[\text{torr}]$. Both capillary ends were open such that gas escapes to the vacuum chamber. During injecting gas, a high voltage of 0-30 kV from the incentive source is

https://doi.org/10.1017/hpl.2023.50 Published online by Cambridge University Press

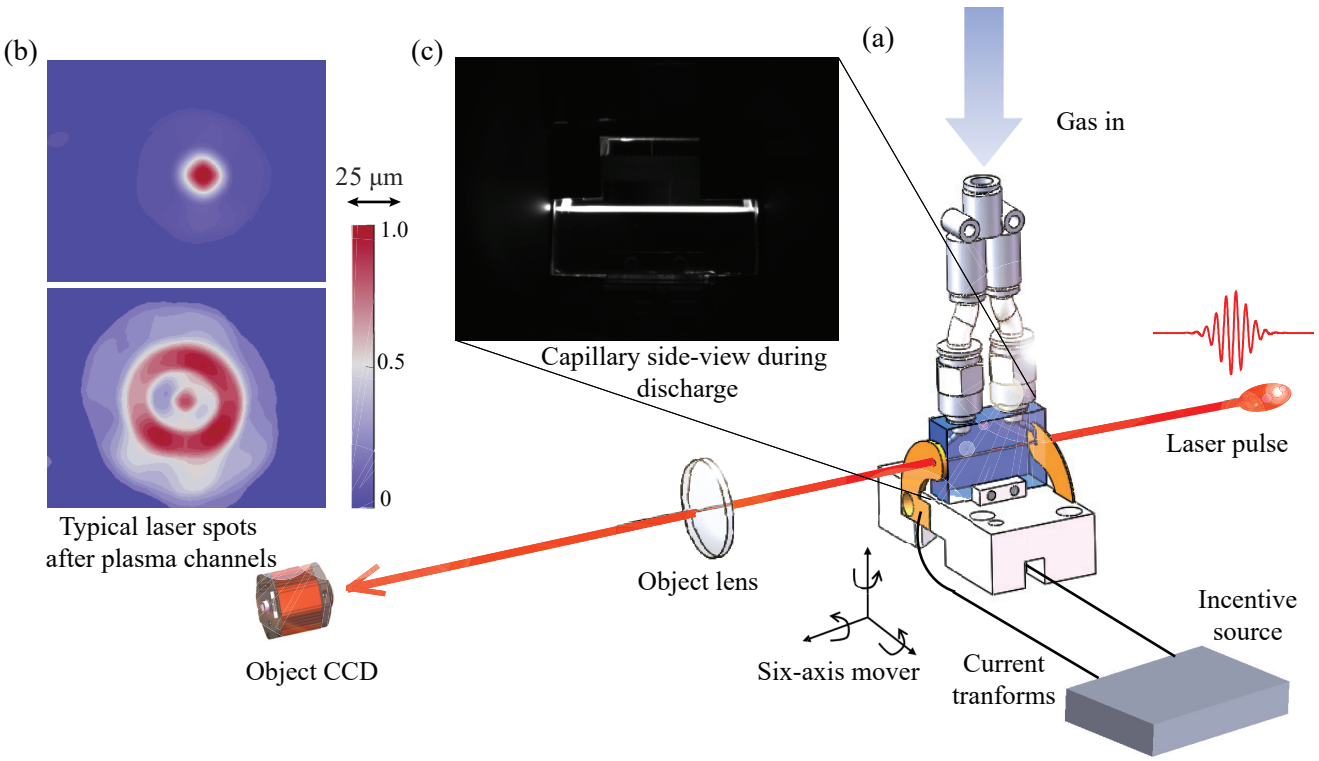

Figure 4. (a) Schematic overview of the experimental setup. Laser pulses propagate from right to left along a capillary as axis $z-$direction. The capillary is carried by a six-axis mover. Gas injects from pipes to fill the capillary. Electrodes connected to the incentive source are located at both ends. The imaging system consisting of a single object lens and CCD is downstream. (b) Typical experimentally measured transverse laser spot intensity distributions at the capillary exit plane during plasma discharge for plasma channels with $\Psi < 0.2$ (the upper subfigure) and $\Psi > 0.5$ (the lower one) respectively. (c) Discharge phenomenon of a gas-filled capillary viewed from the side.

https://doi.org/10.1017/hpl.2023.50 Published online by Cambridge University Press

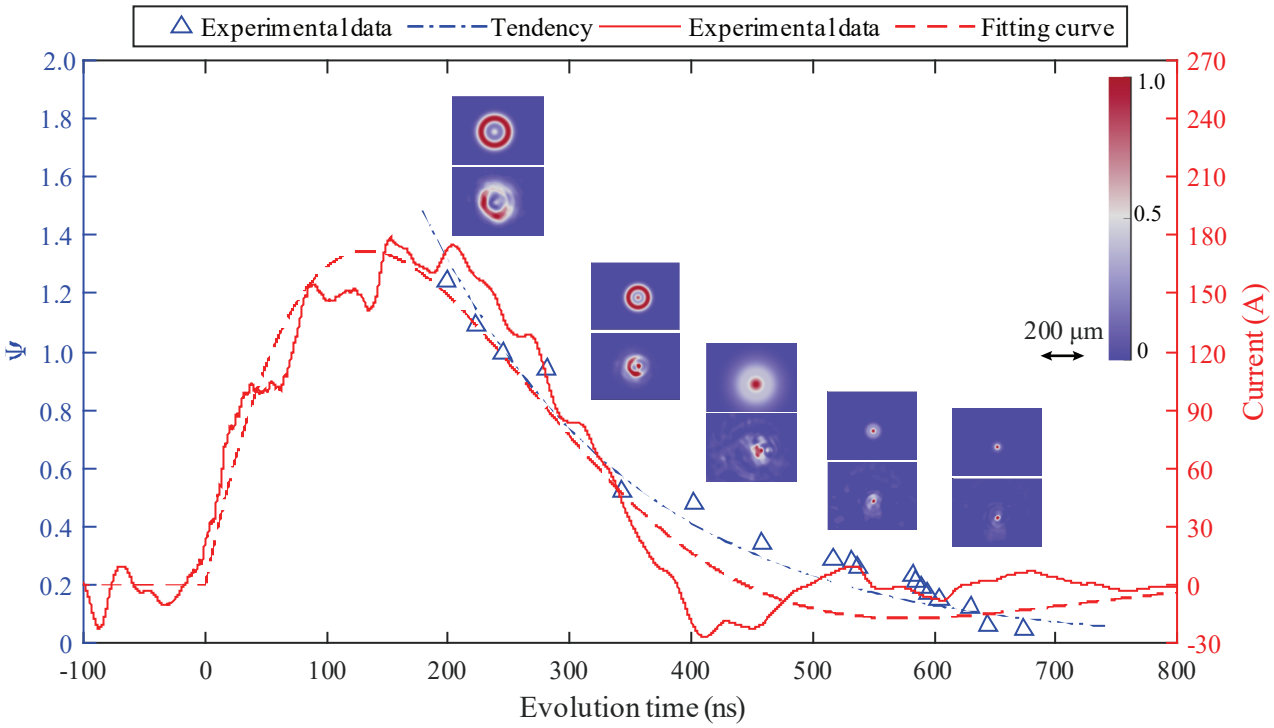

Figure 5. Current waveform measured in No. 9 experiment in a solid red line and fitting results with the waveform based on Eq.19 in a broken red line, reconstructed evolution of Ψ from experimental data in blue triangle marks and an exponential decline tendency of Ψ evolution in a dotted blue line. Both of the red curves above have the *y*-axis on the right in red. Both of the blue curves latter have the *y*-axis on the left in blue. Subfigure groups made up of the lower one, a measured profile, and the upper one, a reconstructed profiles via fitting results, in the same column from left to right correspond to a laser pulse propagating through plasma channels at 245 ns, 343 ns, 458 ns, 537 ns and 644 ns, respectively. And all subfigures are under the unified ruler and color bar placed in the upper left corner inside.

applied to the electrodes located at both ends of the capillary which will lead to gas discharge to generate plasma. A circuit loop is then formed and the plasma is heated to change into a channel by a current pulse with a peak of 100-400 A. Laser pulses can be guided propagating through the channels at probably time windows. Fig.4(c) shows the photo of plasma channel luminescence during discharge of the gas-filled capillary.

A simple lens imaging system is set for this detection. The distance between the lens with a focal length of 25 cm and the capillary outlet is about 30 cm. The transverse, time-integrated laser pulse profile was imaged with a charged-coupled-device (CCD) camera, which has 1600×1200 pixels and a resolution of 0.517 μm/pixel. Fig.4 (b) shows examples of measured (single shot, background subtracted) transverse laser pulse intensity distributions at the location of the capillary exit aperture. The upper one represents typical laser spots, which are almost transversely Gaussian, downstream across plasma channel density profiles with $\Psi < 0.2$, where the quartic density contributions can be negligible. And the lower one represents those which is no longer fundamental model Gaussian, with $\Psi > 0.5$ where the quartic density contributions are obvious in the initial process of plasma channel evolutions, generally.

A DG645 device was used to achieve that laser pulses with a repetition rate of 1 kHz propagate through discharged plasma channels at various times, by allocating delay times of the thyratron switch trigger signal referring to the regenerative amplifier trigger signal. The thyratron switch in the incentive source is triggered to close with several ns time jitter. Helmholtz coils are set around current transform cables to get the discharge current time-evolving waveforms and a photodiode was used to get signals when laser pulses arrived. Both two can be measured by an oscilloscope at the same time. The relative time difference between the timing moments of two waveforms is the basis for the time relationship between a laser pulse and a plasma channel.

All the experimental parameter groups are listed in Tab.1. As an example, the result of No. 9 experiment will be analyzed follow shown in Figure.5. The technique adopted in our incentive is the simple RLC circuit. The selectable ranges of resistors (R), inductances (L) and capacitors (C) are 0-500 Ω, 0-18 μH and 0.5-30 nF, respectively. A principle $R^2 \approx 2L/C$ followed makes the current waveform, shown in Fig.5 by the solid red line, approximate to a single sine pulse to suppress electromagnetic impacts from the discharge on

https://doi.org/10.1017/hpl.2023.50 Published online by Cambridge University Press

electronic equipment, which can be described as a form

$$I = I_0 e^{-\alpha t} \sin\omega t \ \ (t > 0) \tag{19}$$

where α and ω are decline and oscillation time scale respectively. The fitting curve shown in Fig.5 based on Eq.19 of the current waveform can provide the time origin of discharge. The CCD is synchronously triggered by the DG645 device and is able to acquire the transverse, time-integrated intensity profile of the laser pulses. The Quasi-Newton Algorithm[99] and the model identification technique[100] can be studied to fit the intensity images with Eq.15. Two rows of subfigures are respectively experiential profiles (lower ones) and reconstructed profiles via fitting results (upper ones) in Fig.5, where the intensity is normalized. Notice that the pulse is no longer transversely fundamental Gaussian. The subfigure groups (both two in every column) from left to right correspond to a laser pulse propagating through plasma channels at 245 ns, 343 ns, 458 ns, 537 ns and 644 ns, respectively. And the unified ruler and color bar are placed in the upper left corner inside Fig.5. The blue triangle marks are coefficients Ψ defined in Sev.2 reconstructed from fitting results with the experimental measurements. It is almost certain there is an exponential decline tendency $e^{-\varsigma t}$ of Ψ, which indicates that r^4 density contribution decreases in the whole current heating process. It is related to the current drop from the peak over time. The coefficient ς can be defined as a time-dependent decline rate to denote the decrease rate of Ψ i.e., the contribution of a quartic density profile. For the case in Fig.5, $\varsigma = 5.72\ \mathrm{s}^{-1}$ from the fitted dotted blue line.

5. Experimental results and discussions

In previous work, the impact of discharge voltages and avalanche process[101] on the development of subsequent plasma channels was rarely considered. Here, we evaluated the influence of the discharge voltages on plasma density evolution with quartic distributions by three styles of waveforms with different current pulse widths keeping the peak currents the same as much as possible shown in Figure.6 (a). The three different styles of waveforms are obtained by adjusting circuit parameters R, L and C simultaneously. It is difficult to ensure the same current waveform. Only if the high voltage V of Style 1, Style 2 and Style 3 is respectively 20 kV, 18 kV and 15 kV, the peaks are almost equal i.e., that of NO.9, NO.10 and NO.1 experimental groups. The waveform oscillation time scale ω can be reconstructed as 6.985 $\mu\mathrm{s}^{-1}$, 2.764 $\mu\mathrm{s}^{-1}$ and 0.017 $\mu\mathrm{s}^{-1}$ respectively, which is a highly discriminative parameter. But for such short current pulses, characteristic parameters of the current transmission loop strongly depend on the current itself. Gas-filled capillaries are enough small loads to neglect. The plasma channel-guided effect starts almost between 200-300 ns after the current time origin.

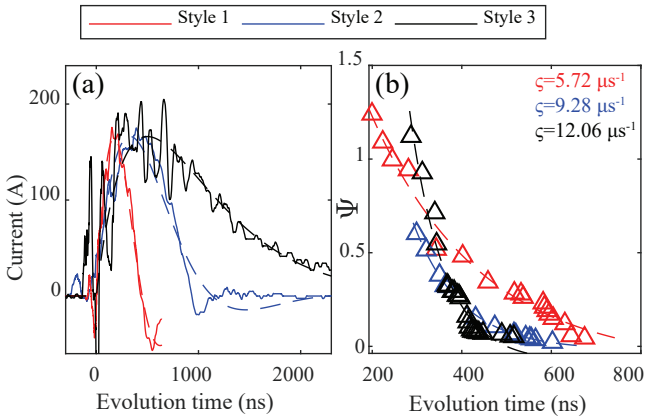

Figure 6. (a) Measured in solid lines and fitting in broken lines current waveforms of Style 1 in red, Style 2 in blue and Style 3 in black with ω = 6.985 $\mu\mathrm{s}^{-1}$, 2.764 $\mu\mathrm{s}^{-1}$ and 0.017 $\mu\mathrm{s}^{-1}$ respectively in NO.9, NO.10 and NO.1 experiments correspondingly. (b) Reconstructed evolutions of density profile coefficient Ψ in triangle marks and exponential decline tendencies in broken lines with various styles of waveforms in NO.9 (red), NO.10 (blue) and NO.1 (black) experiments.

At the rising edge of the current, the gas is rapidly broken down and transformed into almost fully ionized plasma. Discharge voltages positively push the process via more electron emissions[101]. From around the current peak moment, the non-uniform plasma profile is formed and begins to evolve. The evolution process is positively correlated with the current resulting in the heating effect. In order to evaluate the impact of the breakdown on the evolution, we manipulated the incentive source to generate plasma in waveform with a higher voltage but a smaller heating current, i.e. a steeper falling edge of the current. The decline ς of Ψ still decreases with the current, shown in Fig.6 (b), which infers that the gain from voltages is not enough to offset the reduction in current and the impact of the breakdown can be negligible compared to current heating.

For the same style of waveform with almost one same oscillation scale ω, currents are almost positively linearly related to voltages. In the experiments with a same style waveform, the circuit parameters R, L and C is fixed and adjusting voltages would make peak currents change. In the following analysis of the influences, it would be clear that the effect from currents is dominant compared to voltages.

In order to clarify the influence of experimental conditions on the profile evolutions, we would adopt the control variable method for group comparisons listed in Tab.1. Figure.7 (a) shows reconstructed profile evolutions in triangle marks and exponential decline tendencies in broken lines with various high voltage V=15 kV, 20 kV, 25 kV and 28 kV respectively in red, blue, black and green correspondingly in NO.1, NO.2, NO.3 and NO.4 experiments for He plasma. And Fig.7 (b) shows those in NO.5, NO.6, NO.7 and NO.8 experiments for Ar plasma. Both Fig.7(a) and (b) evidence that ς increases

https://doi.org/10.1017/hpl.2023.50 Published online by Cambridge University Press

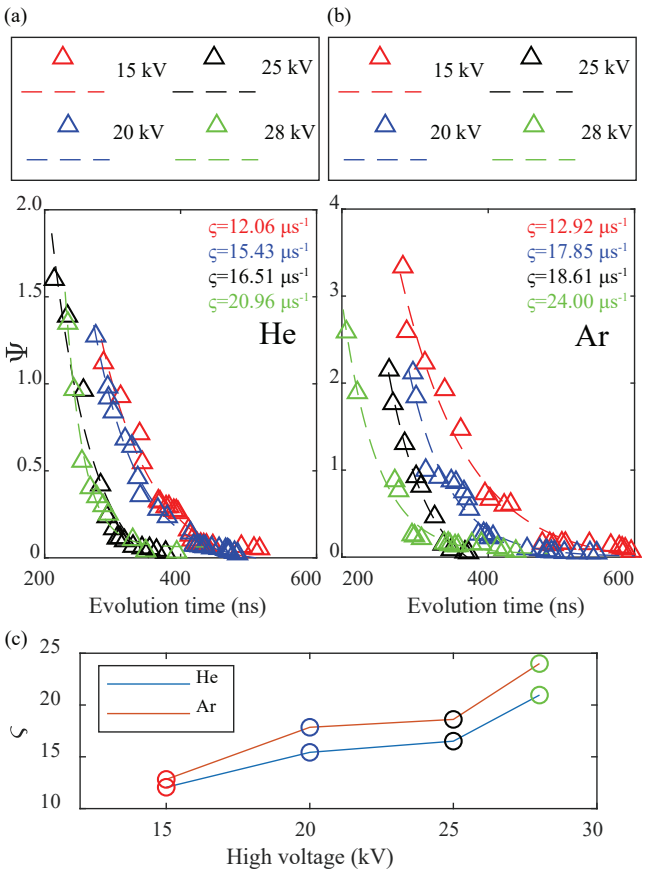

Figure 7. Reconstructed evolutions of density profile coefficient Ψ in triangle marks and exponential decline tendencies in broken lines (a) with various high voltages V =15 kV, 20 kV, 25 kV and 28 kV for He plasma in NO.1 (red), NO.2 (blue), NO.3 (black) and NO.4 (green) experiments, (b) with various high voltages V =15 kV, 20 kV, 25 kV and 28 kV for Ar plasma in NO.5 (red), NO.6 (blue), NO.7 (black) and NO.8 (green) experiments. (c) Scaling of exponential decline rate ς with high voltages for He plasma in the light-blue line and Ar plasma in the light-red line. The circle marks is in colors corresponding to those in (a) and (b)

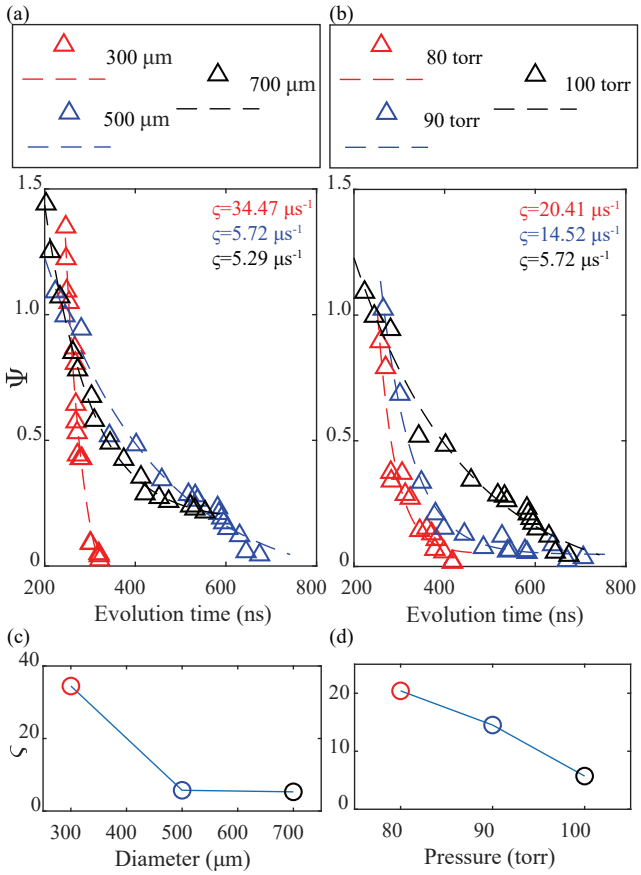

Figure 8. Reconstructed evolutions of density profile coefficient Ψ in triangle marks and exponential decline tendencies in broken lines (a) with various capillaries diameters d = 300 μm, 500 μm, 700 μm in NO.11 (red), NO.9 (blue) and NO.12 (black) experiments, and (b) with various pressures p =80 torr, 90 torr, 100 torr in NO.13 (red), NO.14 (blue) and NO.9 (black) experiments. (c) Scaling of exponential decline rate ς with diameters. The circle marks is in colors corresponding to those in (a). (d) Scaling of exponential decline rate ς with pressures. The circle marks is in colors corresponding to those in (b).

https://doi.org/10.1017/hpl.2023.50 Published online by Cambridge University Press

with voltages increasing, essentially that is an increase in the heating effect of the current, which is shown in Fig.7 (c). Meanwhile, they also evidence that ς of Ar plasma is larger than that of He plasma shown in Fig.7 (c). One can be interpreted as that the discharge of Ar plasma is accompanied by weaker electron-ion heat conduction[45].

Figure.8 (a) shows reconstructed profile evolutions in triangle marks and exponential decline tendencies in broken lines with various capillary diameters d=300 μm, 500 μm and 700 μm respectively in red, blue and black correspondingly in NO.11, NO.9 and NO.12 experiments, which evidences that ς increases with diameters decreasing shown in Fig.8 (c). Fig.8 (b) shows reconstructed profile evolutions in triangle marks and exponential decline tendencies in broken lines with various capillary pressures P=80 torr, 90 torr and 100 torr respectively in red, blue and black correspondingly in NO.13, NO.14 and NO.9 experiments, which evidences that ς increases with pressures decreasing shown in Fig.8 (d). The capillary load is small enough, so the difference in parameters of capillaries themselves hardly affects the circuit characteristics. It is a widely held view that current densities depending on diameters and plasma densities depending on pressures are important factors for local plasma heating. When the current is the same, less plasma will be heated to a higher temperature in less time. Besides, more advanced techniques are needed to address the starting moment of the channel-guided effect experimentally. The problem brings some disturbance to the analysis.

From the experimental results, we can roughly describe the phenomenon of the plasma channel evolution. Previous research work[67,68,93] has described the Ohmic heating model of plasmas under quasi-thermal equilibrium conditions. It is the basis that the $J-T$ model[67] is well suited for parabolic density distributions. We could consider that the parabolic density distribution indicated by the model $n(r)/n_0 = 1 + ar^2/r_{ch}^2$ is approximately valid when $\Psi \to 0$, where a is a main current-related parameter that needs to be measured[68]. A rough evolution hypothesis can be described by the conservation of the number of particles $\partial \langle n \rangle / \partial t = 0$ in the plasma channel. The evolution is from a significant quartic density distribution to a parabolic density distribution holding average constant. However, the approximation is limited as the sub-microsecond timescale is close to the characteristic timescale of acoustic velocity.

So far, the quartic density profile evolution at the outer edge of the channel has not been succinctly described as a brief model. We suspect that this has a lot to do with heat conduction, nonlocal-thermal-equilibrium, potential balance, and particle collisions and diffusion with the wall material. Probably, it is a reasonable explanation to associate quartic density profile contributions with the plasma presheath of arc discharges[102]. Due to the conservation of particle number, the density at outer edge of channels is positively correlated with the plasma temperature

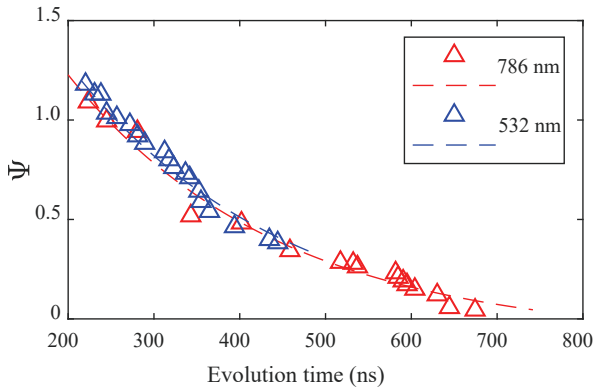

Figure 9. Reconstructed profile evolutions in triangle marks and exponential decline tendencies in broken lines from measurements with laser wavelength λ=786 nm of the front (red) end and λ=532 nm of a Q-switch laser (blue), respectively.

in the central channel region. And obviously, the same goes for temperature at edge. Thus, the thickness of presheath negatively correlated with temperature. In this way, the profile evolution process is linked to the initial temperature rise of the central plasma. To a certain extent, Ψ and ς would physically express temperature and temperature rate, respectively. It is possible to introduce why voltages and currents are positive factors to quicken plasma evolutions, and electron-ion heat conduction, radii and pressures are negative. We consider that quickening plasma evolutions is equivalent to increasing the exponential decline tendency coefficient ς of the rate Ψ of quartic density contribution

The density profile evolution offers additional ideas for optimizing the plasma channel. For applications of capillaries such as guiding ultra-intense laser pulses and laser-plasma acceleration, ideal parabolic density profiles seem to require sufficient plasma heating but within larger temperature gradients. The laser-plasma relativistic interactions considering quartic profile contributions remain unstudied. For charged particle beam transports with plasma channels as APLs, the current density profile is a crucial factor. Plasma with almost entirely parabolic distributions and large temperature gradients is not conducive to maintaining beam emittance. Far from quasi-thermal equilibrium conditions, the impact of quartic profile contributions on the current density profile is unknown. A balance should be found on whether to change circuit parameters or to choose different plasma synchronous moments, when searching for the desired currents.

One more experiment has been carried out with the same contributions but laser wavelength λ=532 nm in NO.9 experiment. We deployed a Q-switched laser. Equations.12 -16 do not exhibit a significant dependence on wavelength. Figure.9 confirms this. The reconstructed profile evolution measured by the laser pulses from the front end in red triangle marks and the Q-switched laser in blue ones have a good consistency. The trigger of the latter is subjected to

https://doi.org/10.1017/hpl.2023.50 Published online by Cambridge University Press

severe electromagnetic shock from the plasma discharges, resulting in a shorter time window for measurements. The slight difference between the two tendencies comes from the sensitivities of different photodiodes, possibly.

6. Conclusions

Inspired by previous research, we study the channel-guided laser propagation in plasma channels with quartic density profiles. For a given plasma distribution, an approximate intensity evolution of the channel-guided laser is concluded. Under the assumption in the presence of the longitudinal flow and axisymmetric distribution, the laser intensity distribution at the outlet of the fixed-length plasma channel corresponds to the density profile information. The evolution process of a plasma density profile would be given by measurements of transverse, time-integrated laser intensity profiles at various times. We define a characteristic coefficient that is appropriate to describe the problem. In particular, the evolution processes of channel plasma density profiles with quartic density profile contributions may be described as an exponential decline tendency of the coefficients over time. The influence of decline rate donating profile evolution speed, including but not limited to circuit parameters, capillary diameters, types of gases injected and pressures were studied, experimentally. It can be found that voltages and currents are positive factors to quicken plasma evolutions when parameters of the filled gas are held constant, and electron-ion heat conduction, radii and pressures are negative ones, when parameters of the incentive source are held constant. The experimental results in this paper provide support and reflection for the physical research on discharged capillary plasma and optimizing plasma channels in various applications.

Acknowledgement

This work was supported by the National Natural Science Foundation of China (Grants No. 11975037, NO. 61631001 and No. 11921006), and the National Grand Instrument Project (No. 2019YFF01014400 and No. 2019YFF01014404).

References

1. T. Tajima and J. M. Dawson. Laser electron accelerator. *Phys. Rev. Lett.*, 43:267–270, Jul 1979.
2. E. Esarey, P. Sprangle, J. Krall, and A. Ting. Overview of plasma-based accelerator concepts. *IEEE Transactions on Plasma Science*, 24(2):252–288, 1996.
3. E. Esarey, C. B. Schroeder, and W. P. Leemans. Physics of laser-driven plasma-based electron accelerators. *Rev. Mod. Phys.*, 81:1229–1285, Aug 2009.
4. Simon Martin Hooker. Developments in laser-driven plasma accelerators. *Nature Photonics*, 7(10):775–782, 2013.
5. Xiaoming Wang, Rafal Zgadzaj, Neil Fazel, et al. Quasi-monoenergetic laser-plasma acceleration of electrons to 2 gev. *Nature communications*, 4(1):1–9, 2013.
6. Wim P Leemans, Bob Nagler, Anthony J Gonsalves, et al. Gev electron beams from a centimetre-scale accelerator. *Nature physics*, 2(10):696–699, 2006.
7. W. P. Leemans, A. J. Gonsalves, H.-S. Mao, et al. Multi-gev electron beams from capillary-discharge-guided subpetawatt laser pulses in the self-trapping regime. *Phys. Rev. Lett.*, 113:245002, Dec 2014.
8. A. J. Gonsalves, K. Nakamura, J. Daniels, et al. Petawatt laser guiding and electron beam acceleration to 8 gev in a laser-heated capillary discharge waveguide. *Phys. Rev. Lett.*, 122:084801, Feb 2019.
9. R. Weingartner, S. Raith, A. Popp, et al. Ultralow emittance electron beams from a laser-wakefield accelerator. *Phys. Rev. ST Accel. Beams*, 15:111302, Nov 2012.
10. G. R. Plateau, C. G. R. Geddes, D. B. Thorn, et al. Low-emittance electron bunches from a laser-plasma accelerator measured using single-shot x-ray spectroscopy. *Phys. Rev. Lett.*, 109:064802, Aug 2012.
11. Olle Lundh, J Lim, Clément Rechatin, et al. Few femtosecond, few kiloampere electron bunch produced by a laser–plasma accelerator. *Nature Physics*, 7(3):219–222, 2011.
12. Alexander Buck, Maria Nicolai, Karl Schmid, et al. Real-time observation of laser-driven electron acceleration. *Nature Physics*, 7(7):543–548, 2011.
13. JP Couperus, R Pausch, A Köhler, et al. Demonstration of a beam loaded nanocoulomb-class laser wakefield accelerator. *Nature communications*, 8(1):1–7, 2017.
14. CGR Geddes, Cs Toth, J Van Tilborg, et al. High-quality electron beams from a laser wakefield accelerator using plasma-channel guiding. *Nature*, 431(7008):538–541, 2004.
15. Jérôme Faure, Yannick Glinec, A Pukhov, et al. A laser–plasma accelerator producing monoenergetic electron beams. *Nature*, 431(7008):541–544, 2004.
16. Stuart PD Mangles, CD Murphy, Zulfikar Najmudin, et al. Monoenergetic beams of relativistic electrons from intense laser–plasma interactions. *Nature*, 431(7008):535–538, 2004.
17. A. Zigler, Y. Ehrlich, C. Cohen, J. Krall, and P. Sprangle. Optical guiding of high-intensity laser pulses in a long plasma channel formed by a slow capillary discharge. *J. Opt. Soc. Am. B*, 13(1):68–71, Jan 1996.
18. Y. Ehrlich, C. Cohen, A. Zigler, et al. Guiding of high intensity laser pulses in straight and curved plasma channel experiments. *Phys. Rev. Lett.*, 77:4186–4189, Nov 1996.
19. Y. Ehrlich, C. Cohen, D. Kaganovich, et al. Guiding and damping of high-intensity laser pulses in long plasma channels. *J. Opt. Soc. Am. B*, 15(9):2416–2423, Sep 1998.
20. D. Kaganovich, P. V. Sasorov, Y. Ehrlich, et al. Investigations of double capillary discharge scheme for production of wave guide in plasma. *Applied Physics Letters*, 71(20):2925–2927, 1997.
21. D. Kaganovich, A. Ting, C. I. Moore, et al. High efficiency guiding of terawatt subpicosecond laser pulses in a capillary discharge plasma channel. *Phys. Rev. E*, 59:R4769–R4772, May 1999.
22. R. F. Hubbard, Y. Ehrlich, D. Kaganovich, et al. Intense laser pulse propagation in capillary discharge plasma channels. *AIP Conference Proceedings*, 472(1):394–403, 1999.
23. D. Kaganovich, P. Sasorov, C. Cohen, et al. Variable profile capillary discharge for improved phase matching in a laser wakefield accelerator. *Applied Physics Letters*, 75(6):772–774, 1999.
24. Tomonao Hosokai, Masaki Kando, Hideki Dewa, et al. Optical guidance of terrawatt laser pulses by the implosion phase of a fast z-pinch discharge in a gas-filled capillary. *Opt. Lett.*, 25(1):10–12, Jan 2000.

https://doi.org/10.1017/hpl.2023.50 Published online by Cambridge University Press

25. Eric Esarey, Jonathan Krall, and Phillip Sprangle. Envelope analysis of intense laser pulse self-modulation in plasmas. *Phys. Rev. Lett.*, 72:2887–2890, May 1994.
26. E. Esarey, P. Sprangle, J. Krall, et al. Self-focusing and guiding of short laser pulses in ionizing gases and plasmas. *IEEE Journal of Quantum Electronics*, 33(11):1879–1914, 1997.
27. AJ Gonsalves, Kei Nakamura, Chen Lin, et al. Tunable laser plasma accelerator based on longitudinal density tailoring. *Nature Physics*, 7(11):862–866, 2011.
28. Manuel Kirchen, Sören Jalas, Philipp Messner, et al. Optimal beam loading in a laser-plasma accelerator. *Phys. Rev. Lett.*, 126:174801, Apr 2021.
29. N. H. Matlis, A. J. Gonsalves, S. Steinke, et al. Transient behavior of a supersonic three-dimensional micronozzle with an intersecting capillary. *Journal of Applied Physics*, 119(7):074501, 2016.
30. Lucas Schaper, Lars Goldberg, Tobias Kleinwächter, et al. Longitudinal gas-density profilometry for plasma-wakefield acceleration targets. *Nuclear Instruments and Methods in Physics Research Section A: Accelerators, Spectrometers, Detectors and Associated Equipment*, 740:208–211, 2014. Proceedings of the first European Advanced Accelerator Concepts Workshop 2013.
31. N. H. Matlis, A. J. Gonsalves, S. Steinke, et al. Dynamics and density distributions in a capillary-discharge waveguide with an embedded supersonic jet. *Journal of Applied Physics*, 118(20):204506, 2015.
32. Matthias Fuchs, Raphael Weingartner, Antonia Popp, et al. Laser-driven soft-x-ray undulator source. *Nature physics*, 5(11):826–829, 2009.
33. A. Butler, A. J. Gonsalves, C. M. McKenna, et al. Demonstration of a collisionally excited optical-field-ionization xuv laser driven in a plasma waveguide. *Phys. Rev. Lett.*, 91:205001, Nov 2003.
34. Min Chen, Ji Luo, Fei-Yu Li, et al. Tunable synchrotron-like radiation from centimeter scale plasma channels. *Light: Science & Applications*, 5(1):e16015–e16015, 2016.
35. E.A. Gibson, Xiaoshi Zhang, T. Popmintchev, et al. Extreme nonlinear optics: attosecond photonics at short wavelengths. *IEEE Journal of Selected Topics in Quantum Electronics*, 10(6):1339–1350, 2004.
36. J. Luo, M. Chen, W. Y. Wu, et al. Multistage coupling of laser-wakefield accelerators with curved plasma channels. *Phys. Rev. Lett.*, 120:154801, Apr 2018.
37. Kazuhisa Nakajima. Seamless multistage laser-plasma acceleration toward future high-energy colliders. *Light, Science & Applications*, 7, 2018.
38. A. Zigler, M. Botton, Y. Ferber, et al. Consolidating multiple femtosecond lasers in coupled curved plasma capillaries. *Applied Physics Letters*, 113(18):183505, 2018.
39. V. Shpakov, M. P. Anania, M. Bellaveglia, et al. Longitudinal phase-space manipulation with beam-driven plasma wakefields. *Phys. Rev. Lett.*, 122:114801, Mar 2019.
40. R. D'Arcy, S. Wesch, A. Aschikhin, et al. Tunable plasma-based energy dechirper. *Phys. Rev. Lett.*, 122:034801, Jan 2019.
41. R Pompili, D Alesini, MP Anania, et al. Energy spread minimization in a beam-driven plasma wakefield accelerator. *Nature Physics*, 17(4):499–503, 2021.
42. J. van Tilborg, S. Steinke, C. G. R. Geddes, et al. Active plasma lensing for relativistic laser-plasma-accelerated electron beams. *Phys. Rev. Lett.*, 115:184802, Oct 2015.
43. R. Pompili, M. P. Anania, M. Bellaveglia, et al. Experimental characterization of active plasma lensing for electron beams. *Applied Physics Letters*, 110(10):104101, 2017.
44. J. van Tilborg, S. K. Barber, C. Benedetti, et al. Comparative study of active plasma lenses in high-quality electron accelerator transport lines. *Physics of Plasmas*, 25(5):056702, 2018.
45. Carl A Lindstrøm, Erik Adli, G Boyle, et al. Emittance preservation in an aberration-free active plasma lens. *Physical review letters*, 121(19):194801, 2018.
46. R. Pompili, M. P. Anania, M. Bellaveglia, et al. Focusing of high-brightness electron beams with active-plasma lenses. *Phys. Rev. Lett.*, 121:174801, Oct 2018.
47. R. Pompili, G. Castorina, M. Ferrario, et al. Guiding of charged particle beams in curved capillary-discharge waveguides. *AIP Advances*, 8(1):015326, 2018.
48. A. Ferran Pousa, A. Martinez de la Ossa, R. Brinkmann, et al. Compact multistage plasma-based accelerator design for correlated energy spread compensation. *Phys. Rev. Lett.*, 123:054801, Jul 2019.
49. R. Pompili, E. Chiadroni, A. Cianchi, et al. Plasma lens-based beam extraction and removal system for plasma wakefield acceleration experiments. *Phys. Rev. Accel. Beams*, 22:121302, Dec 2019.
50. S. K. Barber, J. H. Bin, A. J. Gonsalves, et al. A compact, high resolution energy, and emittance diagnostic for electron beams using active plasma lenses. *Applied Physics Letters*, 116(23):234108, 2020.
51. Tong Yang, Hao Cheng, Yang Yan, et al. Designing of active plasma lens for focusing laser-plasma-accelerated pulsed proton beams. *Phys. Rev. Accel. Beams*, 24:031301, Mar 2021.
52. Jianhui Bin, Lieselotte Obst-Huebl, Jian-Hua Mao, et al. A new platform for ultra-high dose rate radiobiological research using the bella pw laser proton beamline. *Scientific reports*, 12(1):1–15, 2022.
53. Phillip Sprangle and Eric Esarey. Interaction of ultrahigh laser fields with beams and plasmas. *Physics of Fluids B: Plasma Physics*, 4(7):2241–2248, 1992.
54. P. Sprangle, E. Esarey, J. Krall, et al. Propagation and guiding of intense laser pulses in plasmas. *Phys. Rev. Lett.*, 69:2200–2203, Oct 1992.
55. P. Sprangle, B. Hafizi, and J. R. Peñano. Laser pulse modulation instabilities in plasma channels. *Phys. Rev. E*, 61:4381–4393, Apr 2000.
56. Pallavi Jha, Navina Wadhwani, Ajay. K. Upadhyaya, et al. Self-focusing and channel-coupling effects on short laser pulses propagating in a plasma channel. *Physics of Plasmas*, 11(6):3259–3263, 2004.
57. E. Esarey, C. B. Schroeder, B. A. Shadwick, et al. Nonlinear theory of nonparaxial laser pulse propagation in plasma channels. *Phys. Rev. Lett.*, 84:3081–3084, Apr 2000.
58. C. Ren, B. J. Duda, R. G. Hemker, et al. Compressing and focusing a short laser pulse by a thin plasma lens. *Phys. Rev. E*, 63:026411, Jan 2001.
59. P. Sprangle, J. R. Peñano, and B. Hafizi. Propagation of intense short laser pulses in the atmosphere. *Phys. Rev. E*, 66:046418, Oct 2002.
60. Ajay K. Upadhyay, Gaurav Raj, Rohit K. Mishra, et al. Nonlinear propagation of sinusoidal pulse laser beam in homogeneous plasma. *Physics of Plasmas*, 14(9):093107, 2007.
61. Ajay K. Upadhyay, Gaurav Raj, Rohit K. Mishra, et al. Propagation of sinusoidal pulse laser beam in a plasma channel. *Physics of Plasmas*, 14(11):113105, 2007.
62. P. Sprangle, A. Ting, and C. M. Tang. Radiation focusing and guiding with application to the free electron laser. *Phys. Rev. Lett.*, 59:202–205, Jul 1987.
63. P. Sprangle, A. Ting, and C. M. Tang. Analysis of radiation

https://doi.org/10.1017/hpl.2023.50 Published online by Cambridge University Press

focusing and steering in the free-electron laser by use of a source-dependent expansion technique. *Phys. Rev. A*, 36:2773–2781, Sep 1987.
64. Julien Derouillat, Arnaud Beck, Frédéric Pérez, Tommaso Vinci, M Chiaramello, Anna Grassi, M Flé, Guillaume Bouchard, I Plotnikov, Nicolas Aunai, et al. Smilei: A collaborative, open-source, multi-purpose particle-in-cell code for plasma simulation. *Computer Physics Communications*, 222:351–373, 2018.
65. E. Esarey and W. P. Leemans. Nonparaxial propagation of ultrashort laser pulses in plasma channels. *Phys. Rev. E*, 59:1082–1095, Jan 1999.
66. L Yu, H M Zhao, Q Cao, X Z Zhu, J L Li, B Y Li, F Liu, M Chen, and Z M Sheng. Guiding of laguerre–gaussian pulses in high-order plasma channels. *Plasma Physics and Controlled Fusion*, 64(7):075009, jun 2022.
67. N. A. Bobrova, A. A. Esaulov, J.-I. Sakai, et al. Simulations of a hydrogen-filled capillary discharge waveguide. *Phys. Rev. E*, 65:016407, Dec 2001.
68. B. H. P. Broks, K. Garloff, and J. J. A. M. van der Mullen. Nonlocal-thermal-equilibrium model of a pulsed capillary discharge waveguide. *Phys. Rev. E*, 71:016401, Jan 2005.
69. D. J. Spence and S. M. Hooker. Investigation of a hydrogen plasma waveguide. *Phys. Rev. E*, 63:015401, Dec 2000.
70. David M. Gaudiosi, Brendan Reagan, Tenio Popmintchev, et al. High-order harmonic generation from ions in a capillary discharge. *Phys. Rev. Lett.*, 96:203001, May 2006.
71. D. J. Spence, P. D. S. Burnett, and S. M. Hooker. Measurement of the electron-density profile in a discharge-ablated capillary waveguide. *Opt. Lett.*, 24(14):993–995, Jul 1999.
72. D. J. Spence and S. M. Hooker. Investigation of a hydrogen plasma waveguide. *Phys. Rev. E*, 63:015401, Dec 2000.
73. Fernando Brandi and Leonida Antonio Gizzi. Optical diagnostics for density measurement in high-quality laser-plasma electron accelerators. *High Power Laser Science and Engineering*, 7:e26, 2019.
74. A. J. Gonsalves, T. P. Rowlands-Rees, B. H. P. Broks, et al. Transverse interferometry of a hydrogen-filled capillary discharge waveguide. *Phys. Rev. Lett.*, 98:025002, Jan 2007.
75. T. G. Jones, A. Ting, D. Kaganovich, et al. Spatially resolved interferometric measurement of a discharge capillary plasma channel. *Physics of Plasmas*, 10(11):4504–4512, 2003.
76. J. Kim, V. L. J. Phung, K. Roh, et al. Development of a density-tapered capillary gas cell for laser wakefield acceleration. *Review of Scientific Instruments*, 92(2):023511, 2021.
77. Y. Ping, I. Geltner, A. Morozov, et al. Interferometric measurements of plasma density in microcapillaries and laser sparks. *Physics of Plasmas*, 9(11):4756–4766, 2002.
78. Han S. Uhm, Dong G. Jang, Min S. Kim, et al. Density dependence of capillary plasma on the pressure and applied voltage. *Physics of Plasmas*, 19(2):024501, 2012.
79. G. Bagdasarov, P. Sasorov, A. Boldarev, et al. Plasma equilibrium inside various cross-section capillary discharges. *Physics of Plasmas*, 24(5):053111, 2017.
80. J. M. Garland, G. Tauscher, S. Bohlen, et al. Combining laser interferometry and plasma spectroscopy for spatially resolved high-sensitivity plasma density measurements in discharge capillaries. *Review of Scientific Instruments*, 92(1):013505, 2021.
81. A. Curcio, F. Bisesto, G. Costa, et al. Modeling and diagnostics for plasma discharge capillaries. *Phys. Rev. E*, 100:053202, Nov 2019.
82. Zhu Xin-Zhe, Li Bo-Yuan, Liu Feng, et al. Experimental study on capillary discharge for laser plasma wake acceleration. *Acta Physica Sinica*, 71(9):095202, 2022.
83. A. Biagioni, M.P. Anania, M. Bellaveglia, et al. Electron density measurement in gas discharge plasmas by optical and acoustic methods. *Journal of Instrumentation*, 11(08):C08003, aug 2016.
84. Pavel S. Antsiferov, Mohamed R. Akdim, and Herman T. van Dam. Direct measurement of the matched spot size in a slow capillary discharge optical waveguide. *Review of Scientific Instruments*, 78(12):123107, 2007.
85. Jiaqi Liu, Wentao Li, Jiansheng Liu, et al. Measurement of the matched spot size in a capillary discharge waveguide with a collimated laser. *AIP Advances*, 8(10):105204, 2018.
86. T. P. Rowlands-Rees, C. Kamperidis, S. Kneip, et al. Laser-driven acceleration of electrons in a partially ionized plasma channel. *Phys. Rev. Lett.*, 100:105005, Mar 2008.
87. T. G. Jones, K. Krushelnick, A. Ting, et al. Temporally resolved raman backscattering diagnostic of high intensity laser channeling. *Review of Scientific Instruments*, 73(6):2259–2265, 2002.
88. J. Daniels, J. van Tilborg, A. J. Gonsalves, et al. Plasma density diagnostic for capillary-discharge based plasma channels. *Physics of Plasmas*, 22(7):073112, 2015.
89. J. van Tilborg, A. J. Gonsalves, E. H. Esarey, et al. Density characterization of discharged gas-filled capillaries through common-path two-color spectral-domain interferometry. *Opt. Lett.*, 43(12):2776–2779, Jun 2018.
90. J. van Tilborg, A. J. Gonsalves, E. Esarey, et al. High-sensitivity plasma density retrieval in a common-path second-harmonic interferometer through simultaneous group and phase velocity measurement. *Physics of Plasmas*, 26(2):023106, 2019.
91. A. J. Gonsalves, K. Nakamura, C. Lin, et al. Plasma channel diagnostic based on laser centroid oscillations. *Physics of Plasmas*, 17(5):056706, 2010.
92. M. Turner, A. J. Gonsalves, S. S. Bulanov, et al. Radial density profile and stability of capillary discharge plasma waveguides of lengths up to 40 cm. *High Power Laser Science and Engineering*, 9:e17, 2021.
93. B H P Broks, J van Dijk, H M J Bastiaens, et al. Study of a pulsed capillary discharge waveguide with a modulated radius. *Journal of Physics D: Applied Physics*, 39(11):2384, may 2006.
94. E. Esarey, P. Sprangle, J. Krall, et al. Self-focusing and guiding of short laser pulses in ionizing gases and plasmas. *IEEE Journal of Quantum Electronics*, 33(11):1879–1914, 1997.
95. Victor V Kotlyar and Alexey A Kovalev. Nonparaxial propagation of a gaussian optical vortex with initial radial polarization. *JOSA A*, 27(3):372–380, 2010.
96. Anthony E Siegman. *Lasers*. University science books, 1986.
97. A. D. Buckingham and C. Graham. The density dependence of the refractivity of gases. *Proceedings of the Royal Society of London. Series A, Mathematical and Physical Sciences*, 337(1609):275–291, 1974.
98. J. G. Zhu, M. J. Wu, Q. Liao, et al. Experimental demonstration of a laser proton accelerator with accurate beam control through image-relaying transport. *Phys. Rev. Accel. Beams*, 22:061302, Jun 2019.
99. Roger Fletcher. *Practical Methods Of Optimization: Vol. 1 Unconstrained Optimization*. John Wiley & Sons, 1980.
100. Xudong Yuan, Yaguang Xu, Ruizhi Zhao, et al. Dual-output mode analysis of multimode laguerre-gaussian beams via deep learning. *Optics*, 2(2):87–95, 2021.
101. MJ Druyvesteyn and Fi M Penning. The mechanism of electrical discharges in gases of low pressure. *Reviews of Modern Physics*, 12(2):87, 1940.

https://doi.org/10.1017/hpl.2023.50 Published online by Cambridge University Press

102. B Mancinelli, Leandro Prevosto, JC Chamorro, et al. Modelling of the plasma–sheath boundary region in wall-stabilized arc plasmas: Unipolar discharge properties. *Plasma Chemistry and Plasma Processing*, 38(1):147–176, 2018.
103. T D Arber, K Bennett, C S Brady, et al. Contemporary particle-in-cell approach to laser-plasma modelling. *Plasma Physics and Controlled Fusion*, 57(11):113001, sep 2015.

https://doi.org/10.1017/hpl.2023.50 Published online by Cambridge University Press